EINDHOVEN UNIVERSITY OF TECHNOLOGY

Structural properties of Bi containing InP films explored by cross-sectional scanning

Citation for published version (APA):
Krammel, C. M., Koenraad, P. M., Roy, M., Maksym, P. A., & Wang, S. (2019). Structural properties of Bi containing InP films explored by cross-sectional scanning. In S. Wang, & P. Lu (Eds.), *Springer Series in Materials Science* (pp. 215-229). (Springer Series in Materials Science; Vol. 285). Springer. https://doi.org/10.1007/978-981-13-8078-5_10

Document license:
TAVERNE

DOI:
10.1007/978-981-13-8078-5_10

Document status and date:
Published: 01/01/2019

Document Version:
Accepted manuscript including changes made at the peer-review stage

Please check the document version of this publication:

• A submitted manuscript is the version of the article upon submission and before peer-review. There can be important differences between the submitted version and the official published version of record. People interested in the research are advised to contact the author for the final version of the publication, or visit the DOI to the publisher's website.
• The final author version and the galley proof are versions of the publication after peer review.
• The final published version features the final layout of the paper including the volume, issue and page numbers.

Link to publication

General rights
Copyright and moral rights for the publications made accessible in the public portal are retained by the authors and/or other copyright owners and it is a condition of accessing publications that users recognise and abide by the legal requirements associated with these rights.

• Users may download and print one copy of any publication from the public portal for the purpose of private study or research.
• You may not further distribute the material or use it for any profit-making activity or commercial gain
• You may freely distribute the URL identifying the publication in the public portal.

If the publication is distributed under the terms of Article 25fa of the Dutch Copyright Act, indicated by the “Taverne” license above, please follow below link for the End User Agreement:

www.tue.nl/taverne

Take down policy
If you believe that this document breaches copyright please contact us at:

openaccess@tue.nl

providing details and we will investigate your claim.

Download date: 05. Oct. 2023

Structural properties of Bi containing InP films explored by cross-sectional scanning tunneling microscopy

C. M. Krammel, P. M. Koenraad, M. Roy, P. A. Maksym, and S. M. Wang

Abstract The structural properties of highly mismatched III-V semiconductors with small amounts of Bi are still not well understood at the atomic level. In this chapter, the potential of cross-sectional scanning tunneling microscopy (X-STM) to address these questions is reviewed. Special attention is paid to the X-STM contrast of isovalent impurities in the III-V system, which is discussed on the basis of theoretical STM images of the (110) surface using density functional theory (DFT) calculations. By comparing high-resolution X-STM images with complementary DFT calculations, Bi atoms down to the third monolayer below the InP (110) surface are identified. With this information, the short range ordering of Bi is studied, which reveals a strong tendency towards Bi pairing and clustering. In addition, the occurrence of Bi surface segregation at the interfaces of an InP/$InP_{1-x}Bi_x$/InP quantum well with a Bi concentration of 2.4 % is discussed.

C. M. Krammel
Department of Applied Physics, Eindhoven University of Technology, Eindhoven 5612 AZ, The Netherlands, e-mail: c.m.krammel@tue.nl

P. M. Koenraad
Department of Applied Physics, Eindhoven University of Technology, Eindhoven 5612 AZ, The Netherlands e-mail: p.m.koenraad@tue.nl

M. Roy
Department of Physics and Astronomy, University of Leicester, University Road, Leicester LE1 7RH, United Kingdom e-mail: mr6@leicester.ac.uk

P. A. Maksym
Department of Physics and Astronomy, University of Leicester, University Road, Leicester LE1 7RH, United Kingdom e-mail: map@leicester.ac.uk

S. M. Wang
State Key Laboratory of Functional Materials for Informatics, Shanghai Institute of Microsystem and Information Technology, Chinese Academy of Sciences, Shanghai 200050, China e-mail: shumin@mail.sim.ac.cn

1 Background

Since the early days of semiconductor technology alloying has been a popular way to tailor material properties. In the last years, dilute bismides, which belong to the relatively new class of highly mismatched semiconductors, have attracted a lot of attention due to their unusual physical properties [1]. Previous studies have shown that the addition of a dilute amount of Bi atoms to conventional binary III-V semiconductor compounds, such as GaAs and InP, not only leads to a strong reduction of the band gap but also a significant increase of the spin-orbit splitting [2, 3], among other benefits. This can potentially result in a situation where the direct band gap is smaller than the spin-obit splitting. Under such conditions some non-radiative Auger recombination processes are intrinsically suppressed, which makes dilute bismides a promising material for more efficient emitters in the infrared range of the electromagnetic spectrum [4].

Despite considerable efforts to realize Bi containing compounds, little is known about their composition at the atomic scale. In addition, it is difficult to incorporate Bi in III-V semiconductors at typical growth conditions due to the large size of the heavy Bi atoms and the weak III-Bi bond strength. Therefore, bismides are typically synthesized at relatively low growth temperatures and a high Bi/V flux ratio [5]. Under these circumstances, inhomogeneities can arise in the Bi distribution and the formation of crystal defects. Hence, there is a strong need for detailed structure studies that can address these properties. This is essential for a deeper understanding of the mechanism behind the unusually strong influence of Bi on the band structure of its host, which goes beyond the phenomenological band anticrossing (BAC) model [6]. We have used cross-sectional scanning tunneling microscopy (X-STM), which allows the direct imaging nanostructures and impurities below the growth surface without averaging, to address these questions [7].

So far, the majority of experimental efforts have focused on to the growth and physical properties of $GaAs_xBi_{1-x}$ [8, 9]. In contrast, only a few works investigate the microscopic structure of dilute bismides, which are typically performed on Bi containing GaAs layers [10, 11]. These studies are mainly limited to averaging techniques such as scanning transmission electron microscopy (STEM) and extended X-ray absorption fine-structure spectroscopy (EXAFS) measurements, which cannot capture all morphological attributes. Much less is known about Bi in InP, which is another technologically important material system for optoelectronic applications.

In this chapter we provide an in-depth review of our recent X-STM studies on Bi containing InP films and InP_xBi_{1-x}/InP quantum wells (QWs) [7, 12]. First, the concept of X-STM on zinc-blende III-V semiconductors is outlined in section 2. Here, emphasis is put on the sample preparation by *in-situ* cleavage along the $\{110\}$ planes, the structural properties of the cleaved $\{110\}$ surfaces, and the X-STM contrast of isovalent impurities in III-V semiconductors [13]. In section 3, the experimentally observed signatures of Bi atoms down to the second monolayer below cleaved $\{110\}$ surfaces are discussed on the basis of complementary density functional theory (DFT) calculations. Section 4 is dedicated to the structural characteristics of Bi in InP. In particular, the tendency toward Bi pairing and clustering is

assessed. Likewise, we investigate in this context the preference of Bi to segregate during the growth towards the surface. Finally, in section 5, we summarize our work.

2 Cross-sectional scanning tunneling microscopy on III-V semiconductors

Scanning tunneling microscopy and its many variations have fundamentally changed the way we perceive the microcosmos. Over the years, X-STM has proven to be a particularly powerful tool for the characterization of buried nanostructures and single impurities in III-V semiconductors with a zinc blende structure [14]. These materials are preferentially grown along the $\langle 100 \rangle$ and $\langle 111 \rangle$ directions. Brittle fracture through one of the natural $\{110\}$ cleavage planes is an elegant way to reveal a cross-sectional view on the grown epilayers. This is a highly nonlinear process, which still is poorly understood [15]. Particularly in strained samples, it is difficult to reliably expose flat $\{110\}$ surfaces. In the following, we focus on the cleavage of highly mismatched bismides, which are not covered in most of the reviews on X-STM [16, 17, 18, 19]. A general introduction into the subject of STM and its theoretical foundations can be found in various excellent books, e.g. [20, 21, 22].

2.1 Sample preparation and cleavage

Untainted and well-defined surfaces are of central importance for successful STM investigations. Atomically flat planes, which simultaneously provide a cross-sectional view on the grown epilayers of III-V semiconductors, can only be prepared by brittle fracture. However, this approach is solely limited to the non-polar $\{110\}$ planes, which are energetically most favorable. Other crystal facets with higher surface energies are not accessible. In addition, cleavage it is by nature a rather cold way of preparing samples, which preserves the atomic structure. This makes it ideal for STM studies on as-grown III-V semiconductors. In contrast, more traditional cleaning processes, which include various annealing and sputtering steps, have the disadvantage of eroding the treated surfaces.

The $\{110\}$ surfaces oxidize instantaneously under ambient conditions and are very susceptible to contaminations due to the reactive dangling bonds. Therefore, the samples have to be cleaved inside the ultra-high vacuum (UHV) system of the STM. Experimentally, the implementation of a reliable cleavage mechanism for strained semiconductor heterostructures is still challenging in a vacuum chamber with limited room to maneuver and procedures can vary widely between different groups. Figure 1 shows a schematic of the cleavage process in our setup, which works well for Bi containing III-V semiconductors.

Typically, samples are grown on standard p- or n-type substrates to warrant good conductivity at low temperatures of about 5 K. For an X-STM measurement, rect-

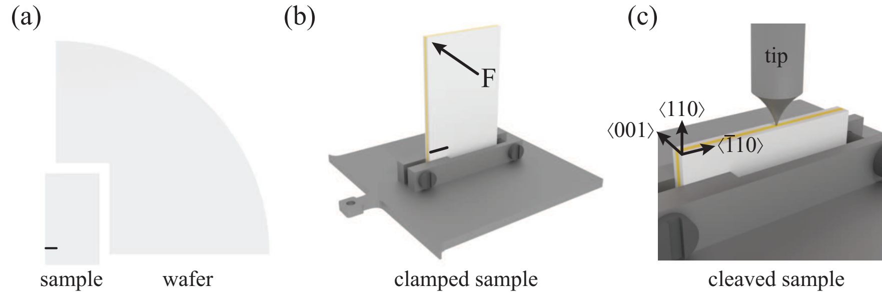

Fig. 1 Schematic representation of the cleavage process: (a) A rectangular X-STM sample of about 5×9 nm^2 is cleaved out of a waver and scratched (black mark) to aid the cleavage process. (b) The sample is vertically mounted into a specially designed vice and cleaved in the UHV system by applying a mechanical force F. (c) The STM tip is in tunnel contact with the exposed epilayers.

angular pieces with an edge length of 4×9 mm^2 are cut out. At the contact points between the sample and the metallic carrier, a Schottky barrier can form. Therefore, ohmic contacts are evaporated on the epilayers in the region of the vice-like clamps. A crucial factor for the cleavage is the thickness of the specimens, which should be as thin as possible. During cleavage, this minimizes the strength of the accumulated strain field, whose energy leads to the formation of surface defects. On the other hand, thinner samples are more susceptible to unintentional cleavages when handling them. The best results are achieved for samples that are thinned down to about 90 μm to 150 μm. This is done by mechanical polishing form the bottom of the substrate, which preserves the epilayers. A scratch across one of the long edges serves as a nucleation point for the cleavage [see black mark in Fig. 1 (a)]. Then, the sample is vertically clamped between two vice-like bars of the sample carrier, as shown in Fig. 1 (b). The bars are designed in such a way that they hold the sample only in the region of the scratch. In this way the crack can propagate more easily along the atomic rows. Inside the STM, the sample is annealed for 25 min at 150 °C to remove water. Just before the X-STM measurement, the sample is cleaved at pressures below 3×10^{-11} mbar by gently touching the corner above the scratch with a wobble stick. This reveals one of the natural $\{110\}$ cleavage planes similar to Fig. 1 (c), which can be imaged with an STM.

2.2 *Properties of the zinc-blende (110) surface*

At the atomic scale, the X-STM contrast is largely governed by the electronic structure of the zinc-blende $\{110\}$ cleavage planes, which have been subject to extensive studies in the last few decades [23, 24, 25, 26]. Therefore, it is crucial to highlight the most important properties of these surfaces.

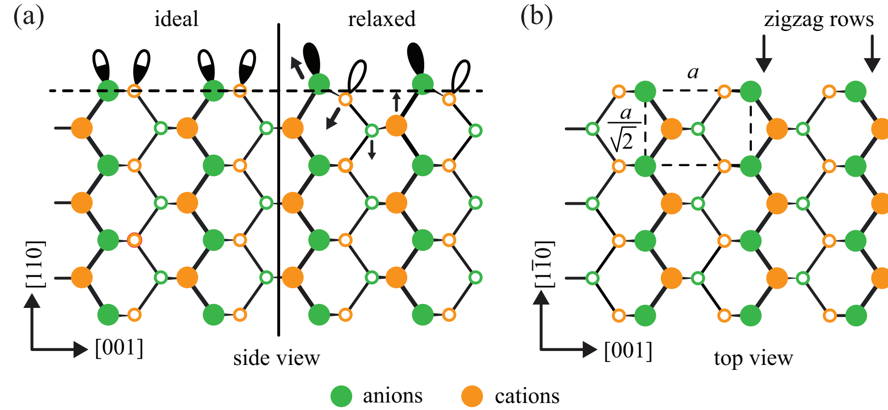

Fig. 2 Schematic ball-and-stick model of the non-polar (110) cleavage plane for a zinc blende crystal where the group III and V elements are represented in orange and green. Atoms in deeper layers are show as rings. (a) In the side view, the arrows indicate the relaxation of the cleaved (110) surface due to the charge redistribution in the originally half filled dangling bonds. (b) In the complementary top view, the primitive 1×1 unit cell and the zig-zag rows are marked. (adapted from Ref. [12])

After cleavage under UHV conditions, the $\{110\}$ surfaces of most III-V semiconductors do not reconstruct. Instead, the group V atoms are shifted outwards away from the crystal while the elements from group III move inwards. This bond rotation, which is indicated by arrows in Fig. 2 (a), conserves the 1×1 unit cell of the bulk $\{110\}$ planes. Lattice sites in the first layer below the surface are only marginally effaced by the buckling. The ideal and relaxed $\{110\}$ surfaces are characterized by zig-zag chains of directly coupled anions and cations, which are separated from each other along the $[001]$ direction by similar chains in the next deeper layer [see Fig. 2 (b)]. By using STM, only the cleavage plane can be imaged, which represents every second layer of the growth front. In addition, the Fermi level is not pinned at clean and defect free $\{110\}$ surfaces in the band gap. In fact, the anionic/cationic surface states, which are centered around the outermost group V/III lattice sites, are resonant with the bulk related valence/conduction bands. At a positive sample voltage electrons tunnel from the metallic tip into the empty surface states in the region of the conduction band, while at a negative sample voltage electrons are extracted from the occupied surface states near the valence band. Thus, it is possible to selectively image the group III and V sublattices under empty and filled state imaging conditions [27].

2.3 *X-STM contrast of isovalent impurities in III-V semiconductors*

STM allows us to visualize different elements in III-V semiconductors at the atomic level. However, a direct chemical sensitivity, which allows for a unique identification of the imaged species is lacking. This means impurities in III-V semiconductors can only be identified through their influence on the local density of states (LDOS) or the surface relaxation. Nevertheless, X-STM is one of the few techniques which allow to probe the bulk like properties of III-V semiconductors at the atomic level. In fact, semiconductor nanostructures and alloys on the basis of (Al, Ga, In)(P, As, Sb) have been extensively studied in the last few decades [28, 29, 30, 31]. In these materials, isovalent impurities from groups III and V typically give rise to atomic-like features, which are either somewhat higher or lower than the surrounding corrugation. For a long time, an in-depth understanding of the physical mechanism, which lies at the bottom of the distinct signatures of single isovalent impurities in X-STM images, has been lacking. It is only recently that Tilley *et al.* used density functional theory (DFT) calculations to systematically assess the X-STM contrast of all isovalent impurities from groups III and V in the GaAs (110) surface [13]. The key observations of this fundamental study are discussed in the following, since they are an important reference point for X-STM measurements on dilute bismides. Experimental X-STM data from other labs on the appearance of Bi atoms in III-V semiconductors are so far hardly available.

The relaxed positions of all stable elements from groups III and V of the periodic table in the GaAs (110) surface, according to first-principles calculations from Tilley and co-workers in Ref. [13], are shown in Fig. 3. The cleaved crystal is most

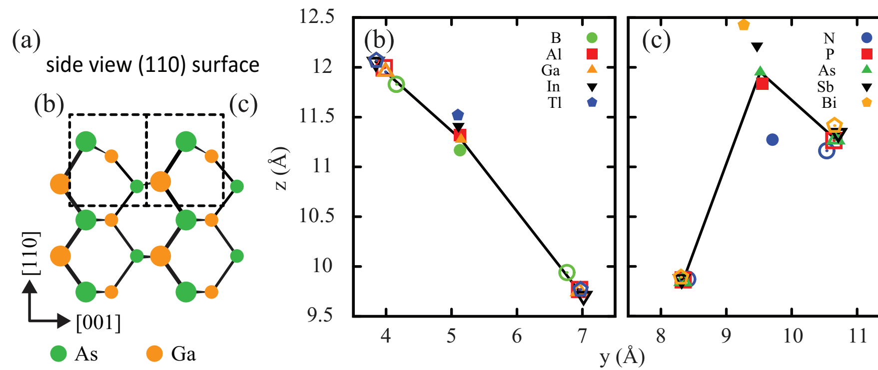

Fig. 3 Comparison of the relaxed positions of all stable elements from groups III and V in the GaAs (110) surface. (a) Schematic side view on the relaxed (110) surface of a zinc-blende crystal where the positions of regions (b) and (c) are highlighted. (b) Shows the relaxed positions of B, Al, Ga, In, Tl from group III and two of their neighboring As atoms. (c) displays the relaxed positions of N, P, As, Sb, Bi from group V and two of their their neighboring Ga atoms. (adapted from Ref. [13])

susceptible to distortions along the [001] directions, which can be best seen in separate side views for all isovalent cations (B, Al, Ga, In, Tl) and anions (N, P, As, Sb, Bi). In both cases, only the impurities (filled symbols) and two of their next nearest nearest neighbors (empty symbols) are plotted, as the lattice displacements decay rapidly in deeper layers. The bucking of the unperturbed GaAs crystal is outlined by black lines, which serve as reference lines. This clearly shows that smaller elements relax into a lower z-position than larger ones. Namely, the P atom lies deeper in the surface than the larger As atom, which it replaces. This effect is even more pronounced at N, which is the smallest element of group V. Conversely, Sb is larger than its substitute and stands out of the surface, which is only topped by the even bigger Bi atom. The same behavior can be found with the elements of group III when going from B to Tl. Due to the bond rotation in the cleavage plane, the modification of the relaxed $\{110\}$ surfaces is stronger for anions than for cations.

In addition, Tilley *et al.* derived from these DFT calculations simulated X-STM images, which allowed them to systematically assess the X-STM contrast of isovalent impurities in the III-V system. Their work clarifies that elements from group III are most easily identified in in empty state images. In Figure 4 (a), impurities

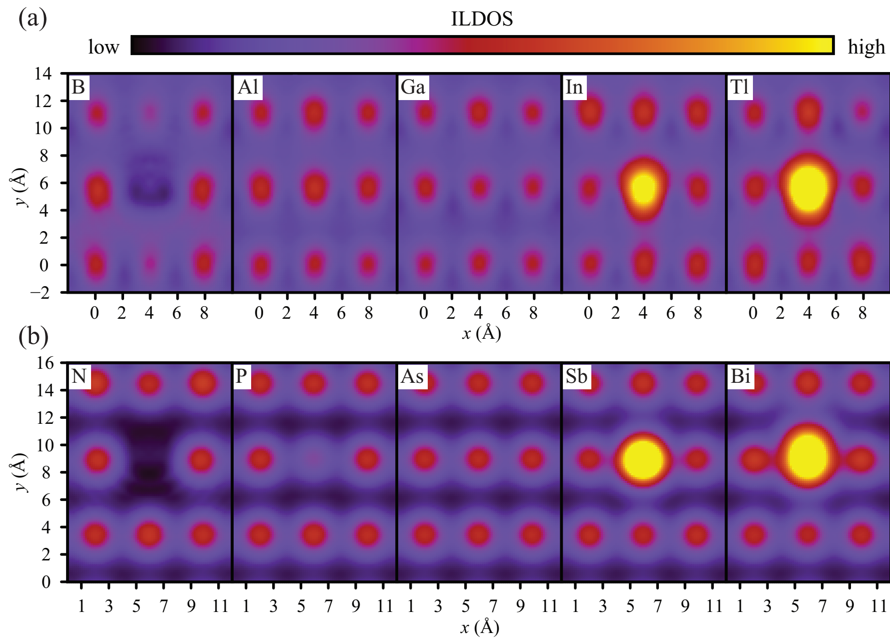

Fig. 4 Simulated STM images for isovalent impurities from groups III and V in the GaAs (110) surface at a constant distance of 4 Å above the unperturbed As atoms. (a) The energy integrated LDOS maps for B, Al, Ga, In, and Tl in the GaAs (110) are calculated for conduction band states up to 1 eV above the band edge. (b) The energy integrated LDOS maps for N, P, As, Sb, and Bi in the GaAs (110) are calculated for valance band states up to 1 eV below the band edge. (adapted from Ref. [13])

with a smaller covalent radius than their substitute give rise to atomic-like dark signatures. In contrast, impurities with a larger covalent radius than their substitute appear as atomic-like bright features. Two exceptions, are Al and Ga, which have almost identical covalent radii. The same trend can be found in simulated filled state images of all stable group V elements from Ref. [13], which are shown in Fig. 4 (b). This shows that the X-STM contrast of isovalent impurities at a large sample voltage reflects primarily structural changes of the relaxed $\{110\}$ surfaces.

3 Spatial structure of individual Bi atoms near the InP (110) cleavage plane

Although X-STM has been extensively used to study conventional semiconductor alloys in the III-V system [18, 32, 33], dilute bismides have received little attention so far. Therefore, it is even more important to provide a thorough discussion of the main Bi related features, which can be found in X-STM measurements at high positive and negative sample voltages. At these conditions, Bi in InP gives rise to three distinct signatures, which represent the local deformation of the surface by Bi atoms down to the second layer below the cleavage plane [7]. Atomically resolved filled state (a, f, k) and empty state (c, h, m) X-STM images of the different Bi related features, which represent the group V and III sublattice respectively, can be found in Fig. 5. Here, energy integrated LDOS maps of the filled valence band (VB) states (b, g, l) and the empty conduction band (CB) states (d, i, n) are shown next to the measurements. A ball-and-stick model on the basis of fully relaxed DFT calculations, which provide a side view on the relaxed (110) surface, can be found in the fifth column of Fig. 5. In these graphs, the unperturbed lattice positions are marked by empty disks. The In, P, and Bi atoms of the relaxed lattice are represented by orange, green, and blue disks, respectively.

The combination of experiment and simulation allows for a depth-dependent identification of Bi atoms near the natural $\{110\}$ cleavage plane. The side view on the fully relaxed crystal in Fig 5 (e), shows that a Bi atom in the cleavage plane, which in the following is called layer 0, stands out of its surrounding in consequence of its large covalent size. This displacement gives rise to an enhanced tunnel current at a constant height above a Bi atom. Therefore, a Bi atom in layer 0 appears in simulated filled and empty state images as an atomic like bright feature, which is either congruent with the group V sublattice or lies between the corrugation of the group III atoms [see Figs. 5 (b, d)]. These simulations are in good agreement with the experimental observations in Figs. 5 (a, c).

A Bi atom in layer 1 has connections to 4 P atoms in the surface, which relax into a higher position in the DFT calculations in Fig. 5 (j). These structural modifications fit well with the rectangular feature in Fig. 5 (f), which is seen in the experiment under filled state conditions. However, in the corresponding simulation the contrast is not as pronounced [see Fig. 5 (g)]. We argue that this discrepancy is due to minor problems with the accuracy of the DFT, which become apparent for the weake fea-

tures induced by Bi. In addition, the deformation of the lattice away from the Bi atom in layer 1 affects primarily one In atom in the cleavage plane. In simulated and experimental empty state images, this gives rise to an atomic-like bright feature [see Figs. 5 (h, i)].

In the second layer below the cleavage plane, the large Bi atom primarily shifts one surface P atom into an higher position. This displacement is not as pronounced as for a Bi atom in layer 0, which in the experimental and simulated filled state X-STM images in Figs. 5 (k, l) gives rise to a weaker atomic like feature than for a Bi atom in the surface. In contrast, the outermost group III elements are much less affected by a Bi atom in layer 2. In the energy integrated LDOS map of the empty CB states in Fig. 5 (n), this leads to a very faint signature similar to the experiment in Fig. 5 (m).

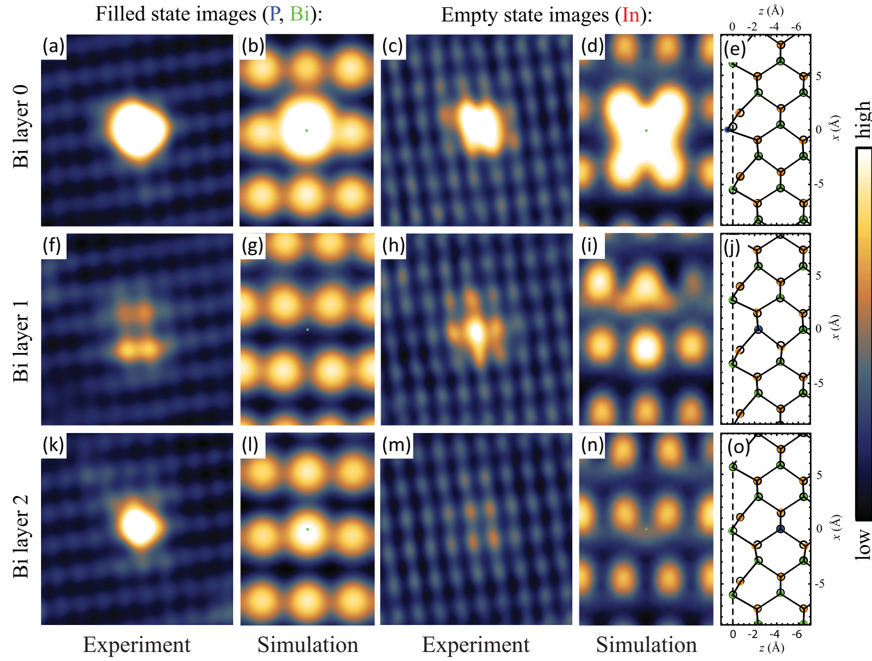

Fig. 5 Identification of the main Bi related features in X-STM measurements on In(P,Bi) films. Topographic filled state images of Bi atoms down to the second layer below the natural cleavage plane, which are taken at $U = -2.4$ V and $I = 30$ pA, are shown in the first column (a, f, k). Complementary empty state topographs, which are acquired at $U = 1.8$ V and $I = 30$ pA, can be found in the third column (c, h, m). Energy integrated LDOS maps of the filled VB states (b, g, l) and empty CB states (d, i, n), which are extracted at a constant height of 4 $\AA$ above the unperturbed P sites, are plotted in a logarithmic scale. In the simulations, either the VB or CB states up to a maximum energy of 1 eV with respect to the band edge are considered. A side view on the relaxed InP (110) surfaces for Bi atoms in the first three layers is provided in the fifth column (e, j, o). In the ball-and-stick plots, the In, P, and Bi atoms are represented by orange, green, and blue disks, respectively. The end of the crystal is indicated by a dashed line. (adapted from Ref. [7])

4 Structural characteristics of Bi containing InP films

At present, the successful incorporation of the large Bi atoms in conventional binary III-V semiconductors remains challenging. Therefore, dilute bismides are still suffering from elemental problems which are related to the ordering of the group V elements [10, 11]. In particular, photoluminescence (PL) measurements on InP films with Bi concentrations up to 2.5 % show unusually strong and broad transitions below the expected band gap [34], which are proposed to be in part related to inhomogeneities in the Bi distribution. Similarly, deep level transient spectroscopy (DLTS) measurements give indications for Bi clustering in InP [35]. Recently, we addressed this topic in an X-STM study on a Bi containing InP sample [7] from the same group that provided the samples for the PL measurements.

4.1 Spatial correlations in the Bi distribution

A typical filled state X-STM image of the investigated InP film with a Bi concentration of 2.4 % is shown in Fig. 6 (a). To quantitatively assess the short range ordering of the Bi atoms relative to each other, we determine for all surface Bi atoms in a surrounding box of 5 × 5 lattice sites the positions of neighboring Bi atoms in the

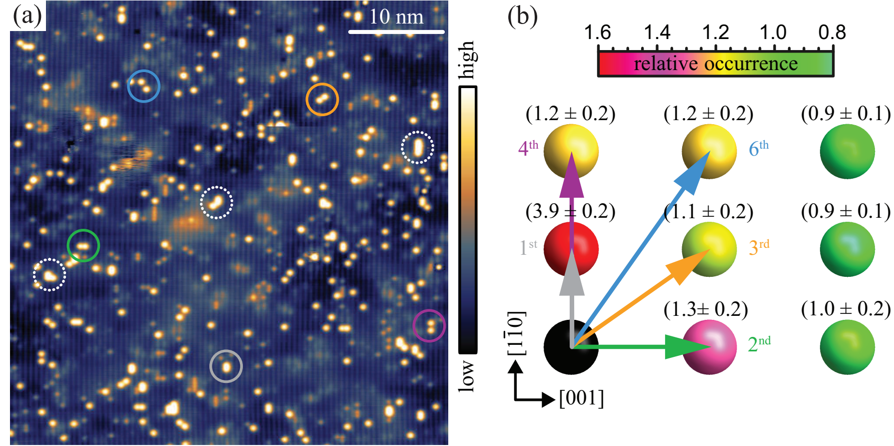

Fig. 6 Irregularities in the local Bi distribution. (a) Topographic filled state X-STM of an InP film with 2.4 % Bi, which is taken $U = -2.6$ V and $I = 40$ pA. 1st, 2nd, 3rd, 4th, and 6th nearest neighbor Bi pairs are indicated with gray, green, orange, purple, and blue circles, respectively. Typical clusters of 3 - 4 Bi atoms are marked by dotted circles. (b) Relative occurrence distribution of the Bi atoms in the natural cleavage plane, which is derived from a $(10.3 \pm 0.2) \times 10^3$ nm^2 large region. The color of the atoms in the 3×3 lattice sites wide grid specifies the probability, compared to a random distribution, of finding additional Bi atoms in a certain range around a reference Bi atom at the black reference position. (adapted from Ref. [7])

cleavage plane. This allows us to define a local occupation matrix for every Bi atom whose elements symbolize its surrounding group V lattice. Here, positions with a Bi atom are represented by 1 and P atoms by 0. Thus, the sum over all local occupation matrices, which are extracted from a $(10.3 \pm 0.2) \times 10^3$ nm^2 large area, provides a measure for the global Bi distribution. These data are normalized by the expectation for a random particle distribution with the same size and particle density as in the experiment. A value larger/smaller than one points to an over-/underpopulation with Bi atoms. The results of this analysis are summarized in form of a 3×3 lattice sites wide grid of the group V elements in the cleavage plane, which is displayed in Fig. 6 (b). In the lower left corner (black sphere) lies the reference position. Further details on this analysis can be found in the supplementary material of Ref. [7]. The calculations show that there is an enhanced probability of finding in the first shell around a Bi atom a second Bi atom. The formation of first nearest neighbor Bi pairs is with a relative occurrence of (3.9 ± 0.2) strongly favorable. The next widest second neighbor Bi pairs with a relative frequency of (1.3 ± 0.2), are only slightly overpopulated. Examples of the five closest n-th Bi-pairs with n = 1, 2, 3, 4, 6 are marked in Fig. 6 (b) with solid circles. On the log range the Bi atoms are randomly distributed within the errors.

In addition to pairs, small clusters which rarely consist of more than 3 atoms are frequently observed at a Bi concentration of 2.4 %. Commonly observed trimers all have a first nearest neighbor pair in common, which typically leads to the triangular, kinked, and linear configuration shown in Fig. 7. This points to a connection with the strong trend toward first nearest neighbor Bi pairing. Similarly, among the three different trimer configurations, linear arrangements are, when compared to the expectations from a random distribution, stronger overpopulated than triangular and kinked geometries. This supports DLTS and PL measurements on Bi containing InP, which also point towards Bi clustering [34, 35].

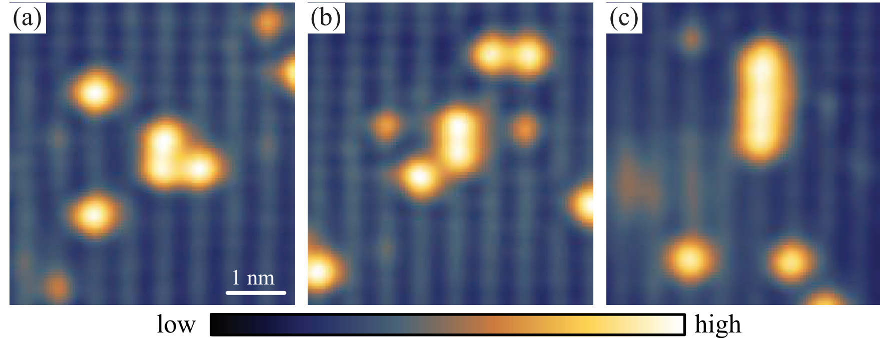

Fig. 7 Examples of commonly observed Bi cluster configurations. The spectrum ranges primarily from triangular (a) to kinked (b), and linear (c) Bi cluster geometries, which are imaged under filled state conditions at $U = -2.5$ V and $I = 40$ pA. (adapted from Ref. [7])

4.2 *Bi surface segregation at the interfaces of an InPBi/InP quantum well*

The realization of defect free and sharp hetero interfaces is crucial for the implementation of Bi containing III-V layers in devices, be it on a scientific or industrial level. In particular, Bi is know to act as a surfactant during the growth of conventional binary III-V semiconductors [36, 37]. At rather low growth temperatures in a kinetically limited regime, Bi can be incorporated in InP to some extent [34, 5, 7]. However, structural and compositional information about as-grown In(P,Bi)/InP layers and their interfaces, which clarify the role of Bi surface segregation in this unconventional growth regime, are largely lacking.

To further investigate this, X-STM is used to study the layer-by-layer composition of a 15 nm wide In(P,Bi) quantum well (QW) with an intended Bi concentration of 1 %, which can be seen in Fig. 8 (a) [12]. From the X-STM image, it is difficult to draw a sharp border between the InP barriers and the Bi containing QW. The classification of the Bi related features in section 3 allows the Bi distribution along the [001] growth direction, which lies perpendicular to the QW, to be determined. Figure 8 (b) shows the corresponding Bi concentration profile, which is calculated over a length of 250 nm on the basis of the Bi atoms in layers 0 and 2. The QW is grown without any interruptions at a substrate temperature of 256 °C by providing a constant Bi flux, which ideally results in a rectangular Bi concentration profile. However, at the beginning of the QW growth the Bi content converges in a non-linear manner towards the targeted 1 %, while at the end it comes to a Bi carry

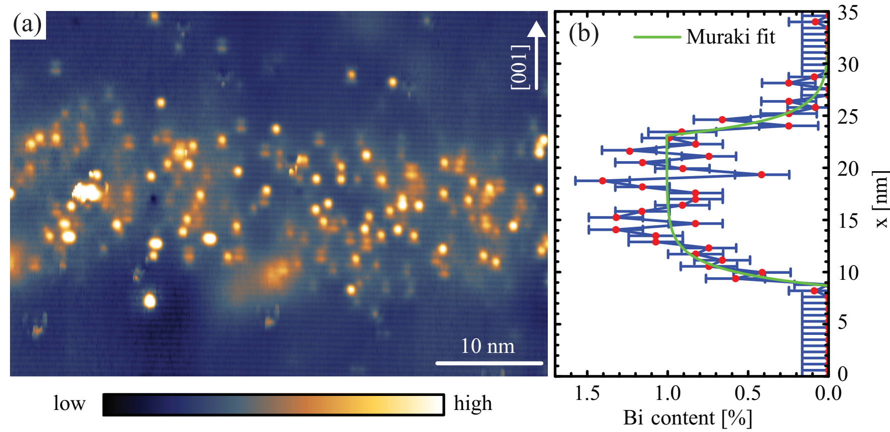

Fig. 8 Bi segregation at the interfaces of a 15 nm wide In(P,Bi) QW, which is surrounded by InP barriers. (a) Topographic filled state image of the QW with a targeted Bi concentration of 1 %, which is acquired at $U = -2.4$ V and $I = 40$ pA. (b) Bi concentration profile along the [001] growth direction, which is determined from a 250 nm long stretch by counting the Bi atoms in layers 0 and 2. The green curve is a fit with Muraki's segregation model [38]. (adapted from Ref. [12])

over. Such a pattern is characteristic for surface segregation where it comes to an exchange between atoms in the surface and the first layer below it. In contrast, Bi diffusion would lead to a symmetric broadening of the concentration profile.

In order to quantify the segregation strength of Bi in the studied QW, the experimentally obtained Bi concentration curve in Fig. 8 (b) is fitted with the empiric model of Murasaki [38]:

$$x_{\mathrm{Bi}}(n) = \begin{cases} 0 & \text{, for } n < N_1 \\ x_0 \left(1 - L^{n-N_1}\right) & \text{, for } N_1 \geq n < N_2 \\ x_0 \left(1 - L^{N_2-N_1}\right) L^{n-N_2} & \text{, for } n \geq N_2 \end{cases} . \tag{1}$$

Here, x_0 represents the nominal Bi concentration in layer n, L is the probability that a Bi atom is transferred to the next layer, N_1 marks the begin of the QW, and N_2 its end. A good fit is obtained for a QW width of (14.4 ± 0.4) nm and a Bi content of $x_0 = (1.01 \pm 0.04)$ %. These parameters come close to the targeted QW thickness of 15 nm at a Bi concentration of 1 %. For the Bi segregation coefficient we obtain $L = (82.9 \pm 3.3)$ %. This value is hard to compare to conventional mixed anion alloys, which are typically grown at much higher temperatures than dilute bismides.

The poor solubility of Bi in zinc blende III-V semiconductors is related to different factors [5, 39]. For example, the incorporation of the large and heavy Bi atoms on substitutional group V sites increases the elastic energy in the crystal. In addition, elemental InBi crystallizes in a PbO configuration while most III-V semiconductors have a zinc-blende structure [40]. At the same time, the In-Bi bond is weaker than the In-P bond [39], which intrinsically favors the incorporation of P over Bi. This triggers Bi surface segregation and makes In(P,Bi) difficult to mix.

There are no simple methods to avoid surface segregation in dilute bismides. One consideration would be to interrupt the growth at the beginning and end of the QW formation, which would give the Bi atoms more time to become incorporated into the crystal. However, this comes at the risk of additional crystal defects at the QW interfaces. Alternatively, an attempt to quickly saturate the surface with Bi atoms could be made by going to a higher Bi flux at the beginning of the QW growth. Similarly, the Bi flux could be lowered towards the end of the QW in order to deplete the Bi reservoir on the growth surface, which is responsible for the Bi tailing.

5 Conclusion

Continuous advances in semiconductor growth technologies have led to the development of novel highly mismatched III-V compounds, such as dilute bismides. These unconventional semiconductors are generally difficult to synthesize due to large miscibility gaps, but offer potentially interesting properties. In particular, little is known about the composition and mixing in In(P,Bi) at the atomic scale. In this chapter, we demonstrate that X-STM is an ideal tool for such investigations.

With the help of complementary DFT calculations, we find that Bi atoms down to the second layer below one of the natural $\{110\}$ cleavage planes affect the relaxed structure of the surface. These characteristic signatures can be measured in topographic filled and empty state X-STM measurements, which are taken at high positive or negative voltages.

Based on this classification the arrangement of the Bi atoms relative to each other is assessed. Interestingly, there is a significantly increased probability of finding first nearest neighbor Bi pairs in InP films with a Bi content of 2.4 %. In addition, the formation of small Bi clusters is observed whose geometries appear to be related to strong first nearest neighbor Bi pairing.

At the interfaces of an In(P,Bi)/InP QW, characteristic signatures in the Bi concentration profile are found, which point to Bi surface segregation. Using the phenomenological segregation model of Muraki *et al*. [38], we find a segregation probability of $L = (82.9 \pm 3.3)$ % at a growth temperature of 256 °C.

References

[1] Y. Zhang, A. Mascarenhas, and L. W. Wang. "Similar and dissimilar aspects of III-V semiconductors containing Bi versus N". In: *Phys. Rev. B* 71 (2005), p. 155201.

[2] Z. Batool et al. "The electronic band structure of GaBiAs/GaAs layers: Influence of strain and band anti-crossing". In: *Journal of Applied Physics* 111 (2012), p. 113108.

[3] X. Chen et al. "Effects of Bi on band gap bowing in $InP_{1-x}Bi_x$ alloys". In: *Opt. Mater. Express* 8 (2018), p. 1184.

[4] Christopher A. Broderick, Muhammad Usman, and Eoin P. O'Reilly. "Theory of the Electronic Structure of Dilute Bismide Alloys: Tight-Binding and $k \cdot p$ Models". In: *Bismuth-Containing Compounds*. Ed. by Handong Li and Zhiming M. Wang. New York, NY: Springer New York, 2013, p. 55. ISBN: 978-1-4614-8121-8.

[5] K. Wang et al. "InPBi Single Crystals Grown by Molecular Beam Epitaxy". In: *Sci. Rep.* 4 (2014), p. 5449.

[6] K. Alberi et al. "Valence-band anticrossing in mismatched III-V semiconductor alloys". In: *Phys. Rev. B* 75 (2007), p. 045203.

[7] C. M. Krammel et al. "Incorporation of Bi atoms in InP studied at the atomic scale by cross-sectional scanning tunneling microscopy". In: *Phys. Rev. Materials* 1 (2017), p. 034606.

[8] S. Francoeur et al. "Band gap of $GaAs_{1-x}Bi_x$, $0 < x < 3.6\%$". In: *Appl. Phys. Lett.* 82 (2003), p. 3874.

[9] S. Tixier et al. "Molecular beam epitaxy growth of $GaAs_{1-x}Bi_x$". In: *Appl. Phys. Lett.* 82 (2003), p. 2245.

[10] D. L. Sales et al. "Distribution of bismuth atoms in epitaxial GaAsBi". In: *Appl. Phys. Lett.* 98 (2011), p. 101902.

[11] G. Ciatto et al. “Spatial correlation between Bi atoms in dilute $GaAs_{1-x}Bi_x$: From random distribution to Bi pairing and clustering”. In: *Phys. Rev. B* 78 (2008), p. 035325.

[12] C. M. Krammel. “Atomic scale investigation of isovalent impurities and nanostructures in III-V semiconductors”. PhD thesis. 2018.

[13] F. J. Tilley et al. “Scanning tunneling microscopy contrast of isovalent impurities on the GaAs (110) surface explained with a geometrical model”. In: *Phys. Rev. B* 93 (2016), p. 035313.

[14] R. M. Feenstra and A. P. Fein. “Scanning tunneling microscopy of cleaved semiconductor surfaces”. In: *IBM J. Res. Develop.* 30 (1986), p. 466.

[15] J K Garleff, a P Wijnheijmer, and P M Koenraad. “Challenges in cross-sectional scanning tunneling microscopy on semiconductors”. In: *Semicond. Sci. Technol.* 26.6 (2011), p. 064001.

[16] A. Mikkelsen and E. Lundgren. “Cross-sectional scanning tunneling microscopy studies of novel IIIV semiconductor structures”. In: *Progress in Surface Science* 80.1 (2005), p. 1.

[17] Edward T. Yu. “Cross-Sectional Scanning Tunneling Microscopy”. In: *Chemical Reviews* 97 (1997), p. 1017.

[18] R. S. Goldman. “Nanoprobing of semiconductor heterointerfaces: quantum dots, alloys and diffusion”. In: *Journal of Physics D: Applied Physics* 37 (2004), R163.

[19] J. K. Garleff, A. P. Wijnheijmer, and P. M. Koenraad. “Challenges in cross-sectional scanning tunneling microscopy on semiconductors”. In: *Semiconductor Science and Technology* 26 (2011), p. 064001.

[20] R. Wiesendanger. *Scanning Probe Microscopy and Spectroscopy: Methods and Applications*. p. 109. Cambridge University Press, 1994. ISBN: 9780521428477.

[21] C. J. Chen. *Introduction to Scanning Tunneling Microscopy*. Oxford Series in Optical and Imaging Sciences. Oxford University Press, 1993. ISBN: 9780198023562.

[22] J. A. Stroscio and W. J. Kaiser. *Scanning Tunneling Microscopy*. Methods of Experimental Physics. Elsevier Science, 1993. ISBN: 9780080860152.

[23] H. Ye et al. “Relaxation models of the (110) zinc-blende III-V semiconductor surfaces: Density functional study”. In: *Phys. Rev. B* 78 (2008), p. 193308.

[24] J. R. Chelikowsky and M. L. Cohen. “Self-consistent pseudopotential calculation for the relaxed (110) surface of GaAs”. In: *Phys. Rev. B* 20 (1979), p. 4150.

[25] Ph. Ebert et al. “Contribution of Surface Resonances to Scanning Tunneling Microscopy Images: (110) Surfaces of III-V Semiconductors”. In: *Phys. Rev. Lett.* 77 (1996), p. 2997.

[26] B. Engels et al. “Comparison between ab initio theory and scanning tunneling microscopy for (110) surfaces of III-V semiconductors”. In: *Phys. Rev. B* 58 (1998), p. 7799.

[27] R. M. Feenstra et al. “Atom-selective imaging of the GaAs(110) surface”. In: *Phys. Rev. Lett.* 58 (1987), p. 1192.

[28] H. A. McKay et al. “Distribution of nitrogen atoms in dilute GaAsN and InGaAsN alloys studied by scanning tunneling microscopy”. In: *J. Vac. Sci. & Technol. B* 19 (2001), p. 1644.

[29] A. Y. Lew et al. “Characterization of arsenide/phosphide heterostructure interfaces grown by gassource molecular beam epitaxy”. In: *Appl. Phys. Lett.* 67 (1995), p. 932.

[30] R. Timm et al. “Contrast mechanisms in cross-sectional scanning tunneling microscopy of GaSb/GaAs type-II nanostructures”. In: *J. Appl. Phys.* 105 (2009), p. 093718.

[31] H. W. M. Salemink, M. B. Johnson, and O. Albrektsen. “Crosssectional scanning tunneling microscopy on heterostructures: Atomic resolution, composition fluctuations and doping”. In: *J. Vac. Sci. & Technol. B* 12 (1994), p. 362.

[32] A. Mikkelsen and E. Lundgren. “Cross-sectional scanning tunneling microscopy studies of novel IIIV semiconductor structures”. In: *Prog. in Surf. Sci.* 80 (2005), p. 1.

[33] Edward T. Yu. “Cross-Sectional Scanning Tunneling Microscopy”. In: *Chem. Rev.* 97 (1997), p. 1017.

[34] X. Wu et al. “Anomalous photoluminescence in $InP_{1-x}Bi_x$”. In: *Sci. Rep.* (2016), p. 27867.

[35] L. Gelczuk et al. “Bi-induced acceptor level responsible for partial compensation of native free electron density in InP 1 x Bi x dilute bismide alloys”. In: *J. Phys. D: Appl. Phys.* 49 (2016), p. 115107.

[36] S. Tixier et al. “Surfactant enhanced growth of GaNAs and InGaNAs using bismuth”. In: *J. Cryst. Growth* 251 (2003), p. 449.

[37] M. R. Pillai et al. “Growth of $In_xGa_{1x}As$/GaAs heterostructures using Bi as a surfactant”. In: *J. Vac. Sci. & Technol. B* 18 (2000), p. 1232.

[38] K. Muraki et al. “Surface segregation of In atoms during molecular beam epitaxy and its influence on the energy levels in InGaAs/GaAs quantum wells”. In: *Appl. Phys. Lett.* 61 (1992), p. 557.

[39] M. A. Berding et al. “Structural properties of bismuth-bearing semiconductor alloys”. In: *J. Appl. Phys.* 63 (1988), p. 107.

[40] L. Dominguez et al. “Formation of Tetragonal InBi Clusters in InAsBi/InAs (100) Heterostructures Grown by Molecular Beam Epitaxy”. In: *Appl. Phys. Exp.* 6 (2013), p. 112601.